Swarming and Swirling in Self-Propelled Polar Granular Rods

Arshad Kudrolli,[1] Geoffroy Lumay,[1,2] Dmitri Volfson,[3] and Lev S. Tsimring[3]
[1]*Department of Physics, Clark University, Worcester, Massachusetts 01610, USA*
[2]*GRASP, Physics Department, University of Liège, B-4000 Liège, Belgium*
[3]*Institute for Nonlinear Science, University of California–San Diego, La Jolla, California 92093, USA*
(Received 16 July 2007; published 8 February 2008)

Using experiments with anisotropic vibrated rods and quasi-2D numerical simulations, we show that shape plays an important role in the collective dynamics of self-propelled (SP) particles. We demonstrate that SP rods exhibit local ordering, aggregation at the side walls, and clustering absent in round SP particles. Furthermore, we find that at sufficiently strong excitation SP rods engage in a persistent swirling motion in which the velocity is strongly correlated with particle orientation.

DOI: 10.1103/PhysRevLett.100.058001 PACS numbers: 45.70.Qj, 05.65.+b

Large-scale structures emerge spontaneously in systems of interacting self-propelled (SP) biological objects such as flocks of birds, schools of fish, amoebae colonies, as well as in multirobot swarms [1,2]. Such observations prompted a discrete-time, discrete-element model by Vicsek *et al.* [3], where SP point particles align their velocities with the average velocity of other particles within a certain fixed-size neighborhood. This model predicts that as the noise (temperature) of the system is reduced below a critical value, the system undergoes a phase transition to a long-range ordered state which appears to be discontinuous in the thermodynamic limit [4]. The Vicsek model was generalized in [5] for SP round particles with an interaction characterized by a Lennard-Jones–type potential and was shown to exhibit gas-liquid and liquid-solid transitions to moving "droplets" and "crystals" of particles.

Further, continuum hydrodynamic-type field models for populations of SP particles have been derived either with general symmetry arguments [6] or directly from microscopic interaction rules [7]. While these models allowed for detailed predictions of the correlation properties within the ordered state, the shape of particles was not taken into account. On the other hand, there have been rapid advances in the theory of "active nematics," or populations of inelastically interacting rods, both polar [8,9] and apolar [10,11]. These models predict the onset of a nematic order when the coupling strength of particle density becomes sufficiently high, and giant density fluctuations in apolar rods. Clustering of polar rods was recently found in numerical simulations [12]. On the experimental side, there has also been growing interest in the nonequilibrium dynamics of driven granular rods. Symmetric rods in a vibrated container have been shown to form nematic or tetratic order and under certain conditions exhibit persistent swirling [11,13,14] and giant number fluctuations [15]. At higher densities, rods bounce on one end and travel in the direction of their tilt due to friction at the contact between the rod and the substrate [16] and collectively form large-scale vortices [17,18].

Here, we study with experiments and simulations, the collective dynamics of vibrated *polar* granular rods that interact only while in contact. The rods have a symmetric shape, but a nonsymmetrical mass distribution which causes them to move toward their lighter end when placed on a vibrating surface. While a single rod reflects off the side walls of the container, a collection of such rods is observed to aggregate over time at the boundaries above a critical excitation. When the magnitude of excitation is increased further, aggregation at the boundaries is reduced, and coherent structures are found in the bulk of the container. Swirls can be identified in time-averaged velocity fields, the flow and the rods are aligned, and signatures of incipient clustering can be observed. To augment these results and extend them toward larger system sizes, we perform numerical simulations using a discrete-element molecular dynamics algorithm. In particular, we show the importance of particle aspect ratio and driving fluctuations on the observed pattern formation.

About 10^3 polar rods were built using white hollow nylon cylinders of length $l = 9.5$ mm and diameter $d = 4.76$ mm, so the aspect ratio of the rods $A_r = l/d$ was fixed at 2 [Fig. 1(a) inset]. Solid steel cylinders of length 4.75 mm and diameter 2.5 mm were placed snugly in one end of the nylon tube, which resulted in the center of mass being displaced by $0.1l$ from the geometrical center of the

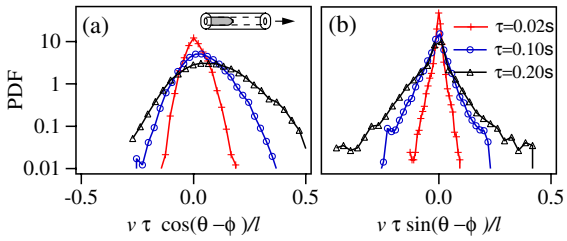

FIG. 1 (color online). The distributions of displacements in a time interval τ (a) parallel and (b) perpendicular to the axis of the polar rod ($\Gamma = 2$). Inset: schematic of the polar rod. The arrow shows the direction of net motion.

rod. The total mass of the assembly was 2.20×10^{-4} kg. The coefficient of friction between the rods, as well as the substrate, is 0.3 ± 0.1. The coefficient of restitution for rod-rod collisions is very difficult to measure; however, the normal coefficient of restitution for spheres of the same material is 0.9. The steel inserts also made the corresponding ends appear somewhat darker and were used to identify the ''polarity'' of the rods. The particles were placed on a flat anodized aluminum container of radius $R = 30d$ vibrated using an electromagnetic shaker with sinusoidal waveform at frequency 75 Hz and varied driving acceleration Γ (scaled by the gravity acceleration) from 0 to 5. A digital camera with the spatial resolution of 1000×1000 pixels was used to image the motion of rods inside the container.

First, we studied the motion of a single rod bouncing on the vibrated plate away from side walls. For $\Gamma > 1.5$, the rod shows a robust net motion in the direction of the lighter end of the rod while taking some apparently random steps in the other directions as well. A movie of the typical motion is contained in the supplementary material [19]. By cross-correlating the intensity distribution of the image of the rod with a mask, we automated finding the position and the orientation (measured by the angle ϕ to a fixed axis) of the rod in each frame. By measuring the change in position over time interval τ, the magnitude of the rod velocity v, and its direction θ with respect to a fixed reference were obtained. The probability distribution functions (PDFs) for the displacement parallel to the rod $v\tau\cos(\theta - \phi)$ and perpendicular to the rod $v\tau\sin(\theta - \phi)$ are plotted in Figs. 1(a) and 1(b) with 3×10^5 sets of measurements. While the PDFs in the perpendicular direction are centered at zero, the broader PDFs in the parallel direction are clearly shifted from zero, and this shift grows as τ is increased. The mean and the root mean square velocity increase with Γ in our system (see supplementary material [19]). By imaging from the side, we find that rods undergo short collisions with the bottom of the container once every few cycles at random phases of the cycle (see supplementary material [19]).

The physical mechanism of the directed motion of polar rods can be understood by extending the arguments developed for symmetric rods and dimers [16,20]. During a typical collision of a particle with a horizontal plate, a large but short impulse of frictional force at the contact point causes horizontal particle displacement after the collision. When a symmetrical (apolar) rod bounces symmetrically on a vibrated plate, the net displacement after many collisions is absent, but for an asymmetric particle, there is a nonzero net horizontal motion. In the case of polar rods, since the center of mass is displaced from the geometrical center, the heavy end collides more often with the plate, and the rod on average travels in the direction of the light end. It can be shown that the average horizontal velocity of the rod translation is proportional to the amplitude of the vertical speed of the container, and indeed we observe that the mean velocity increases with Γ.

The collective motion of polar rods was studied by placing the rods randomly initially inside the container and then vibrating with various Γ. (See the movies included with the supplementary material [19].) For $\Gamma \geq 1.7$, rods were observed to migrate to the boundary of the container and aggregate in about 30 seconds [Fig. 2(a)]. Not all rods aggregate at the boundaries, as some rods gradually rotate and escape from the dense cluster at the boundary back into the middle of the container. For an aspect ratio of 1 (spheres), clustering is not observed at these Γ. As Γ is increased, so do fluctuations, and the aggregation at the boundaries becomes less and less pronounced. Although spatiotemporal density inhomogeneities persist, the time-averaged number density of the polar rods appears more or less uniform across the cavity for $\Gamma > 3$ [Fig. 2(b)].

Next, we performed ''molecular dynamics'' simulations of polar rod motion and interaction. We did not simulate the details of the vibrational transport of bouncing rods, but instead assume that the rods were confined to a horizontal plane. A force acts on each rod along its (horizontal) axis in the direction of the lighter end. This force was assumed to be random, with a mean F and variance V. In addition to the driving force, we assumed that rods experience velocity-dependent friction with the substrate and inelastic collisions with other rods. F and V were tuned so the displacement distribution for a single rod fits the experi-

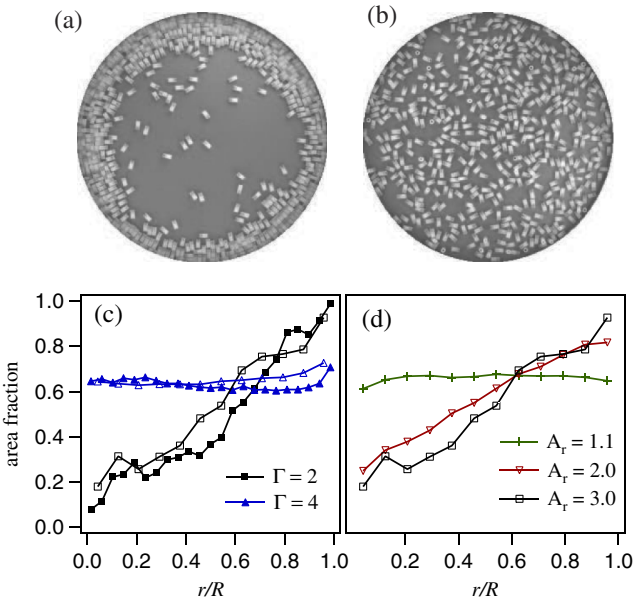

FIG. 2 (color online). (a) Rods migrate and aggregate at the boundaries of a container for modest excitations ($N = 500$, $\Gamma = 2$). (b) Aggregation reduces and a homogeneous distribution is observed as excitation is increased. ($N = 500$, $\Gamma = 4$.) (c) Area fraction $\rho(r/R)$ as a function of distance r from the center of the container with radius R for $N = 900$ averaged over 100 frames at 10 frames per second; open symbols: the results of numerical simulations for the same system parameters; (d) simulations show a decrease of clustering as A_r is reduced ($\Gamma = 2$).

mental data for a given Γ. In the numerics, the rods had a form of spherocylinders, which helped in modeling contact forces. The interaction forces among rods were calculated via the interaction between viscoelastic virtual spheres of diameter d centered at the closest points between the axes of the spherocylinders [16]. Normal forces were computed using the Hertzian spring-dashpot model, and dynamic Coulomb friction was assumed for tangential forces.

We first performed simulations which matched the experiment. We used aspect ratio $A_r = 2$ and imposed elastic boundary conditions on a circle of radius $R_S = 34.2d$ chosen to match the areal density in the experiments. For $F = 0.25$, $V = 0.16$ which corresponds to $\Gamma = 2$, rods tend to aggregate at the boundary in agreement with experiment. As F and V are increased, the aggregation at the boundaries diminishes, also in accord with the experimental observations (see the numerical movies in the supplementary material [19]). To compare the aggregation of rods in the experiments and simulations, we plot the projected rod area fraction ρ as a function of distance from the center r in Fig. 2(c).

Clustering at the walls is not simply a consequence of inelastic collisions. Indeed, it does not occur for small $A_r = 1.1$ [Fig. 2(d)], which indicates that particle shape affects aggregation. When fluctuations are small (at small Γ), rods have a much lower probability of turning around and leaving the wall than spherical particles, and so they are trapped near the wall for a long time.

In order to characterize the density fluctuations inside the container, we computed the standard deviation Δn and the mean n of the number of rods in areas of different sizes [see Fig. 3(a)]. The distributions were obtained by averaging over 1500 frames in the statistically stationary regime, and we restricted the area of measurements to $r/R < 0.7$ to minimize boundary effects. The slope of $\Delta n(n)$ is systematically higher than $\sqrt{n}$. In fact, it is better described by the power $7/12$ which is predicted by the dynamic XY model [6] in the nematic state. At very high values of n the standard deviation drops down, as should be expected since the number of rods becomes comparable with the total number of rods in the container. We also examined a larger system with $R_L = 2.5R_s$ and almost an order of magnitude greater number of rods [Fig. 3(a)]. The deviations from $\sqrt{n}$ are also clearly present in this larger system. It is interesting to contrast these results with "giant" ($\Delta n \sim n$) fluctuations reported for apolar rods [4,10,15]. Although rods in our system have apolar shape, they have mass anisotropy which renders them polar. This polarity appears to destroy the emergence of giant density fluctuations, although greater than $\sqrt{n}$ flucuations showing clustering is observed.

Although global orientational order is clearly absent in our system, there is strong evidence of the local orientational order at sufficiently high density of rods. We can characterize this ordering by computing a local orientational order parameter Q which we define as $Q = \langle \cos 2\Theta \rangle$, where Θ is the angle between directors of a rod and its nearest neighbor and brackets indicate averaging over all

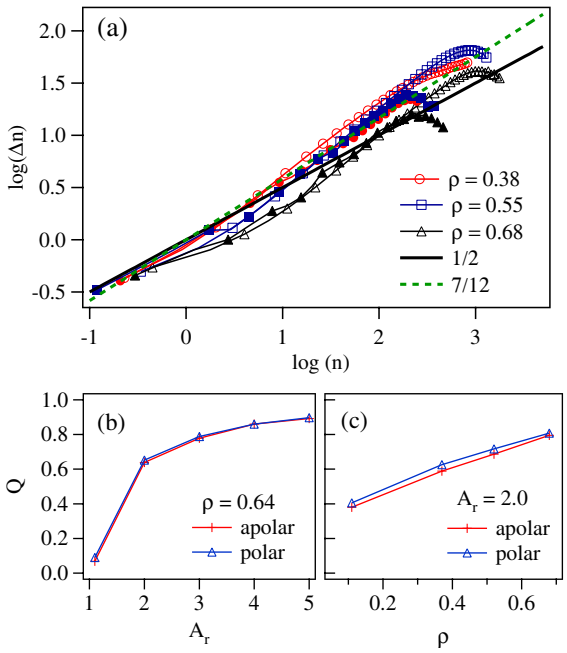

FIG. 3 (color online). (a) The standard deviation of the number of rods Δn versus mean number of rods n inside a circular area at the center of the container ($\Gamma = 3$). Open symbols correspond to the simulations for a larger system size $R_L = 2.5R_S$ but the same density. A fit to the data gives a slope 0.66 ± 0.05, which indicates clustering. (b),(c) Local orientational order parameter Q for nearest neighbors from simulation data for polar and apolar particles as a function of (b) density and (c) aspect ratio.

the rods in the container and time [see Figs. 3(b) and 3(c)]. Parameter Q is similar to the parameter S introduced in [4] and shows significant local orientational order present in our system at high enough ρ and A_r. We carried out similar calculations with apolar particles and found that in the asymptotic regime they exhibit similar (albeit slightly smaller) values of Q. This can be understood since both simulations featured the same magnitude of the fluctuating component of the driving force which created similar "effective temperature" that in turn determined the value of the nematic order parameter. Apparently, the "self-propelled" directed motion of the rods by itself has a small effect on the ordering properties of the system.

Collective motion of rods in the container is masked by the strong random fluctuations, especially at high Γ. To average over fluctuations, we divided the field of view into $2d \times 2d$ boxes and averaged the velocity field over the box area and over a $\tau = 5$ second time interval [Fig. 4(a)]. The velocity field reveals a number of streams and swirls. Numerical simulations for similar parameters also show swirl-like structures [see Fig. 4(b)]. The coherent structures become more pronounced when the system size is increased [Fig. 4(c)]. These structures are reminiscent of swirls obtained with apolar particles driven by the substrate [11,14,21]; however, in that system the mechanism of their generation appears to be rather different.

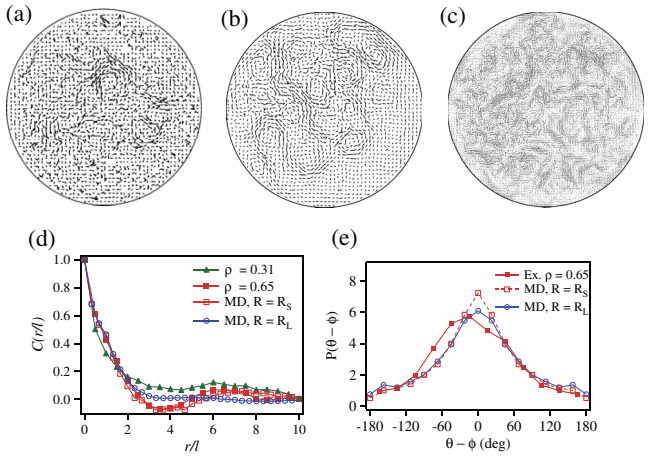

FIG. 4 (color online). Swirling in time-averaged velocity obtained by computing particle displacements after $\tau = 5$ s: (a) experiment ($\Gamma = 3$, $N = 900$), (b) numerics ($F_0 = 1.0$, $\rho = 0.68$), and (c) example of swirls observed in a larger numerical system ($N = 5500$, $R_L = 2.5R_S$). (d) Spatial velocity correlation function $C(r)$ as a function of distance between two rods ($\Gamma = 3$, $\rho = 0.31$, $\rho = 0.65$); results of simulations are shown for small ($R_S = 34.2d$) and large ($R_L = 2.5R_S$) system sizes and for the same density $\rho = 0.68$. (e) The distribution of the angle between rod orientation and its velocity.

To quantify the structure of swirls, we plot in Fig. 4(d) the spatial velocity correlation function $C(r) = \langle \mathbf{v}_1 \cdot \mathbf{v}_2 \rangle / \langle |\mathbf{v}_1||\mathbf{v}_2| \rangle$ for a rod with velocity $\mathbf{v}_1$ and a rod with velocity $\mathbf{v}_2$ separated by distance r. The correlations decay over a distance of a few rod lengths which confirms the lack of the long-range order in the system. However, the structure of the velocity field is strongly correlated with the orientation of the rods. We computed the distribution of the angle between the direction of the velocity field θ in and the mean orientation within a $(2d \times 2d)$ box both in experiment and numerical simulations [Fig. 4(e)]. As seen in Fig. 4(e), there is a significant maximum of this distribution at angle 0, which indicates that rods predominantly move along their axes.

In summary, we have studied the collective dynamics of self-propelled polar rods with experiments and numerical simulations. The phenomenology differs *qualitatively* from that of collective motion of pointlike or round self-propelled particles [4,5] which show no tendency to aggregate near the walls and apolar rods which exhibit giant density fluctuations. We observe aggregation of rods at the boundaries because of the inability of rods to turn around and escape under low noise conditions. As vibration strength and thus noise is increased, the aggregation reduces and a uniformly distributed state displaying local orientational order and swirls are observed. Although our numerical and (especially) experimental studies were conducted in fairly small systems, the accumulation of particles near the boundaries is expected for any closed system. However, whether or not the steady state distribution in the bulk for very large closed systems converges to that for large periodic boundary conditions is an open question. We observe greater than $\sqrt{n}$ density fluctuations which are not accounted for by existing models and deserve further study. In conclusion, our findings elucidate an important and interesting interplay between the shape and the directed motion in *realistic* self-propelled rods which profoundly affects their collective dynamics.

The work was supported by the National Science Foundation under Grant No. DMR-0605664 and by the U.S. Department of Energy under Grant No. DE-FG02-04ER46135.

[1] C. W. Reynolds, Computer Graphics **21**, 25 (1987).
[2] J. Toner, Y. Tu, and S. Ramaswamy, Ann. Phys. (N.Y.) **318**, 170 (2005).
[3] T. Vicsek *et al.*, Phys. Rev. Lett. **75**, 1226 (1995).
[4] G. Grégoire and H. Chaté, Phys. Rev. Lett. **92**, 025702 (2004); H. Chaté, F. Ginelli, and R. Montagne, Phys. Rev. Lett. **96**, 180602 (2006);
[5] G. Grégoire, H. Chaté, and Y. Tu, Physica (Amsterdam) **181D**, 157 (2003).
[6] J. Toner and Y. Tu, Phys. Rev. Lett. **75**, 4326 (1995); J. Toner (personal communication).
[7] E. Bertin, M. Droz, and G. Grégoire, Phys. Rev. E **74**, 022101 (2006).
[8] T. B. Liverpool and M. C. Marchetti, Phys. Rev. Lett. **90**, 138102 (2003); **97**, 268101 (2006); K. Kruse *et al.*, Phys. Rev. Lett. **92**, 078101 (2004).
[9] I. S. Aranson and L. S. Tsimring, Phys. Rev. E **71**, 050901 (2005); **74**, 031915 (2006).
[10] S. Ramaswamy, R. A. Simha, and J. Toner, Europhys. Lett. **62**, 196 (2003); S. Mishra and S. Ramaswamy, Phys. Rev. Lett. **97**, 090602 (2006).
[11] V. Narayan, N. Menon, and S. Ramaswamy, J. Stat. Mech. P01005 (2006).
[12] F. Peruani, A. Deutsch, and M. Bär, Phys. Rev. E **74**, 030904(R) (2006).
[13] J. Galanis *et al.*, Phys. Rev. Lett. **96**, 028002 (2006).
[14] I. S. Aranson, D. Volfson, and L. S. Tsimring, Phys. Rev. E **75**, 051301 (2007).
[15] V. Narayan, S. Ramaswamy, and N. Menon, Science **317**, 105 (2007).
[16] D. Volfson, A. Kudrolli, and L. Tsimring, Phys. Rev. E **70**, 051312 (2004).
[17] D. L. Blair, T. Neicu, and A. Kudrolli, Phys. Rev. E **67**, 031303 (2003).
[18] I. S. Aranson and L. S. Tsimring, Phys. Rev. E **67**, 021305 (2003).
[19] See EPAPS Document No. E-PRLTAO-100-031806 for supplementary movies and material. For more information on EPAPS, see http://www.aip.org/pubservs/epaps.html.
[20] S. Dorbolo, D. Volfson, L. Tsimring, and A. Kudrolli, Phys. Rev. Lett. **95**, 044101 (2005).
[21] I. S. Aranson *et al.*, Phys. Rev. E **75**, 040901 (2007).